

Resonant modes in triangular dielectric cavities

G. M. Wysin*

*Department of Physics
Kansas State University
Manhattan, KS 66506-2601
(Dated: August 12, 2004)*

The resonant optical modes of a high permittivity dielectric prism with an equilateral triangular cross section are discussed. Eigenmode solutions of the scalar Helmholtz equation with Dirichlet boundary conditions, appropriate to a conducting boundary, are applied for this purpose. The particular plane wave components present in these modes are analyzed for their total internal reflection behavior and implied mode confinement when the conducting boundary is replaced by a sharp dielectric mismatch. Improvement in TIR confinement by adjusting the longitudinal wavevector k_z is also discussed. For two-dimensional electromagnetic solutions ($k_z = 0$), TE polarization leads to longer lifetime than TM polarization, assuming that escape of evanescent boundary waves at the corners is the primary decay process.

PACS numbers: 41.20.-q, 42.25.-p, 42.25.Gy, 42.60.-v, 42.60.Da

I. INTRODUCTION

Micro-sized dielectric cavities are becoming increasingly important, due to their applications especially in microlasers and resonators with various geometries, including disks,[1] triangles,[2] squares,[3, 4, 5] and hexagons.[6, 7] Materials where the two-dimensional cross-section controls the properties include, for example, various cleaved semiconductor structures[2] as well as zeolite $ALPO_4-5$ crystals.[6] Even more interesting are lasing semiconductor pyramids that grow by natural processes.[8, 9, 10]

An understanding of the geometry dependence of the total internal reflection (TIR) that produces resonant modes can lead to improvements in designs of optical devices. For the reduced two-dimensional electrostatics (fields independent of a z -coordinate along an axis of symmetry), the boundary element method[11] is very powerful for determining the scattering fields in TM or TE polarizations. Alternatively, here we present a simpler analysis of the resonant modes based only on an analysis of the conditions needed for TIR within a dielectric cavity. The calculation is approximate but simple, especially for a geometry where the related Helmholtz equation has an exact analytic solution.

Here we consider the modes in equilateral triangular-based prisms and their two-dimensional (2D) analogs; the triangular system is chosen here for its interesting symmetries and known analytic Helmholtz solution.[12, 13, 14, 15, 16, 17] As a first approximation, a 2D dielectric system with Dirichlet boundary conditions (DBC) is considered, taking the fields equal to zero at the boundary, equivalent to a metallic or conducting boundary. The exact analytic solutions for this 2D triangular system are

reviewed; each mode is a superposition of only six plane-wave components. We describe how the mode information is useful for determining which modes will be confined if the dielectric is surrounded by a lower index dielectric (or vacuum), rather than a perfect conductor, using the conditions for TIR. A careful analysis shows that when a mode is strongly confined in the cavity by TIR, Dirichlet boundary conditions apply (approximately) to the relevant Helmholtz equation for both the TM and TE polarizations. The simple plane wave components of each mode can be analyzed in terms of Maxwell's equations and the related Fresnel amplitude ratios, which are slightly different for TM and TE polarizations.[18] These differences are shown to imply longer estimated lifetimes for the TE modes, enhanced by a factor of the order of the squared index ratio $(n/n')^2$, when compared to the lifetime of the corresponding TM mode.

Obviously some error is made compared to employing a more technically complete solution of Maxwell's equations such as boundary element methods;[11] the fields discussed here for the dielectric mismatch boundary are not close to the true fields unless the mismatch is very large. This approach, however, should approximately determine the symmetries of the confined modes and give reasonable estimates for the dielectric mismatch needed for their confinements. The improvement of confinement for finite-height prisms with the same cross sections, allowing for nonzero longitudinal wavevector k_z , is also discussed.

II. SIMPLIFIED QUASI-TWO-DIMENSIONAL HELMHOLTZ PROBLEMS

Within a cavity with electric permittivity ϵ and magnetic permeability μ , we consider the solutions of a scalar wave equation for any component ψ of the electric or

*Electronic address: wysin@phys.ksu.edu; URL: <http://www.phys.ksu.edu/~wysin>

magnetic field,

$$\nabla^2 \psi - \frac{\epsilon\mu}{c^2} \frac{\partial^2}{\partial t^2} \psi = 0, \quad (1)$$

where c is the speed of light in vacuum and t is time. The cavity shape being considered is a prism with an equilateral triangular cross-section of edge a in the xy -plane; the height is h along the z axis. Ultimately, we want to discuss which modes will be confined in the cavity of index of refraction $n = \sqrt{\epsilon\mu}$ when it is surrounded by a uniform medium of lower index of refraction $n' = \sqrt{\epsilon'\mu'}$ (for example, vacuum).

We first analyze the modes, assuming the fields go to zero at the cavity walls, using Dirichlet boundary conditions (DBC), which corresponds to perfectly conducting walls, or a mirrored cavity. The range of applicability of these boundary conditions for a mode that is confined by TIR caused by an index mismatch, rather than reflecting boundaries, is discussed subsequently. A solution at frequency Ω is sought, with $e^{-i\Omega t}$ time dependence, corresponding to three-dimensional (3D) wavevectors with magnitude

$$K = \frac{\Omega}{c^*}, \quad c^* = \frac{c}{\sqrt{\epsilon\mu}}; \quad (2)$$

the speed of light in the cavity medium is denoted as c^* . Then we are solving an eigenvalue problem (Helmholtz equation) within the given geometry,

$$\nabla^2 \psi = -K^2 \psi. \quad (3)$$

In the general case, we can consider that we are looking for a superposition of plane waves in the form $e^{i(\vec{K} \cdot \vec{r} - \Omega t)}$, all of which satisfy (3), and with the correct linear combination to satisfy the required boundary conditions. These different components have the same squared wavevector, although they can possess different directions of propagation and different amplitudes. The symmetry of the situation, however, requires only some reduced set of possible wavevectors for triangular-based prisms.

A wavevector is composed from a z -component, k_z , along the vertical or longitudinal axis, and the remaining 2D components in the xy plane, $k^2 \equiv k_x^2 + k_y^2$, so that we decompose the squared magnitude as

$$K^2 = k_z^2 + k^2. \quad (4)$$

Then the frequency is partitioned accordingly,

$$\Omega^2 = \omega_z^2 + \omega^2, \quad (5)$$

where the xy frequency ω and wavevector k are related by an equation analogous to (2), as $k = \omega/c^*$. The remaining part, ω_z , is determined for a prism of height h , assuming some $\psi \propto \sin(k_z z)$ longitudinal dependence, by

$$k_z = \frac{l\pi}{h}, \quad l = 1, 2, 3... \quad (6)$$

which automatically enforces DBC at the ends of the prism. As a result, for the prism geometry, we only solve the separated Helmholtz equation for two dimensions,

$$\nabla_{xy}^2 \psi = -k^2 \psi. \quad (7)$$

A. 2D Electromagnetics at a boundary between media

For 2D E&M problems, which are defined by no dependence of the fields along the prism axis, one takes $k_z = 0$, ignoring any boundary conditions at the prism ends (which can be considered at infinity). Then Maxwell's equations and their associated physical boundary conditions show that one need only consider transverse magnetic (TM) and transverse electric (TE) polarizations of the fields. (Presence of nonzero k_z for a dielectric waveguide surrounded by a different dielectric medium, in general, does not lead to separated TM and TE modes, see Ref. 18.) It is well-known that in a *conducting* waveguide or resonator, at the boundaries of the 2D cross-section, the field $\psi = E_z$ for TM modes satisfies DBC, and the field $\psi = B_z$ for TE modes satisfies Neumann boundary conditions (NBC). Alternatively, if the medium is surrounded simply by a different (nonconducting) dielectric medium, there still are TM or TE polarizations, but, strictly speaking, these would satisfy the more involved boundary conditions of Maxwell's equations, rather than the oversimplified DBC or NBC. If the fields are strongly undergoing TIR (incident angle well beyond the critical angle), however, both polarizations are shown here to satisfy DBC, to a certain limited extent. This can be seen by examining the actual vector fields present under the reflection and refraction at a boundary between two media, for the two possible polarizations.

Consider a planar boundary between two media, where the boundary defines the xz -plane. The region $y < 0$ is occupied by a medium of index $n = \sqrt{\epsilon\mu}$, while the region $y > 0$ is occupied by a medium of index $n' = \sqrt{\epsilon'\mu'}$, with $n > n'$. Primes refer to quantities on the refracted wave side (ultimately, *outside* the system we are studying). The wavevector magnitudes are $k = \frac{\omega}{c} \sqrt{\epsilon\mu}$ and $k' = \frac{\omega}{c} \sqrt{\epsilon'\mu'}$ in the two media. All the waves in this discussion are assumed to have $e^{-i\omega t}$ time dependence. A 2D plane wave $\sim e^{i(k_x x + k_y y)}$ with fields \vec{E}_i, \vec{B}_i , propagating in medium n with $\vec{k}_i = (k_x, k_y) = k(\sin \theta_i, \cos \theta_i)$ and incident on the boundary, can be polarized in two ways, which correspond exactly to the TM and TE polarizations.

Diagrams of the two possible situations are given, for example, in Chap. 7 of Ref. 18. For \vec{E}_i perpendicular to the plane of incidence (xy -plane), $\vec{E}_i = E_i \hat{z}$, and the magnetic field will have no z -component anywhere, which is the same as the TM polarization. On the other hand, for \vec{E}_i lying within the plane of incidence, $\vec{B}_i = B_i \hat{z}$, and the electric field has no z -component anywhere, corresponding to the TE polarization. Thus, we can use the

Fresnel reflection and refraction amplitudes for these two cases, that result from the actual boundary conditions for Maxwell's equations, to investigate the appropriateness of applying DBC for fields undergoing TIR. Furthermore, this analysis will be used for determining the properties of the evanescent refracted wave under TIR; the power lost in this boundary wave can be expected to play a role in the lifetime of a resonant mode.

TM polarization: For incident $\vec{E}_i = E_i^0 \hat{z} e^{i(k_x x + k_y y)}$ perpendicular to the plane of incidence, there is also a reflected wave $\vec{E}_r = E_r^0 \hat{z} e^{i(k_x x - k_y y)}$ with the same polarization, but a different magnitude and phase, depending on the angle of incidence θ_i . One can express the reflected wave amplitude E_r^0 by the Fresnel formula:

$$E_r^0 = E_i^0 e^{-i\alpha}, \quad (8a)$$

$$e^{-i\alpha} = \frac{\sqrt{\frac{\epsilon}{\mu}} \cos \theta_i - \sqrt{\frac{\epsilon'}{\mu'}} \cos \theta'}{\sqrt{\frac{\epsilon}{\mu}} \cos \theta_i + \sqrt{\frac{\epsilon'}{\mu'}} \cos \theta'} \quad (8b)$$

Here θ' is the angle of the refracted wave, obtained from Snell's Law, $n \sin \theta_i = n' \sin \theta'$, which implies TIR when θ_i surpasses the critical angle θ_c , defined by

$$\sin \theta_c = \frac{n'}{n}. \quad (9)$$

Under TIR, E_r^0 has the same magnitude as E_i^0 , but is phase shifted by angle α , because the cosine of the refracted wave becomes pure imaginary:

$$\cos \theta' = i\gamma, \quad \gamma = \sqrt{(\sin \theta_i / \sin \theta_c)^2 - 1}. \quad (10)$$

Then it is useful to express the phase difference between the incident and reflected waves as

$$\tan \frac{\alpha}{2} = \frac{\mu}{\mu'} \sqrt{\frac{\cos^2 \theta_c}{\cos^2 \theta_i} - 1} \quad (11)$$

The linear combination of incident and reflected waves in medium n is $\vec{E} = \vec{E}_i + \vec{E}_r = E_z \hat{z}$, having the spatial variation approaching the boundary (region $y < 0$),

$$E_z = E_i + E_r = 2E_i^0 e^{-i\frac{\alpha}{2}} e^{ik_x x} \cos\left(k_y y + \frac{\alpha}{2}\right) \quad (12)$$

Corresponding to this is the associated evanescent wave in medium n' (region $y > 0$),

$$E_z' = 2E_i^0 e^{-i\frac{\alpha}{2}} e^{ik_x x} e^{-k' \gamma y}, \quad (13)$$

where $k_x = k'_x$ due to Snell's Law. Inspection of Eq. (12) shows that the E_z field on the incident side acquires a node at the boundary $y = 0$ and satisfies Dirichlet BC only when the phase shift attains the value $\alpha = \pi$. According to (11), this occurs only in the limit $\theta_i \rightarrow 90^\circ$, i.e., extreme grazing incidence. Alternatively, at the

threshold for TIR ($\theta = \theta_c$), (11) gives $\alpha = 0$, whereby (12) indicates that the E_z field now will peak at $y = 0$ and satisfies a Neumann BC.

Seeing that the BC on E_z ranges between the two extremes of DBC and NBC, clearly neither boundary condition is fully applicable to the TIR regime. However, it suggests that one should use NBC for finding the TIR threshold conditions, and DBC to determine the field distributions at large enough index mismatch. One can get some indication of the crossover to DBC-like behavior by locating the incident angle $\theta_i = \tilde{\theta}$ where the phase shift passes $\frac{\pi}{2}$, i.e., when $\tan \frac{\alpha}{2} = 1$. From (11) one finds

$$\cos \tilde{\theta} = \frac{\cos \theta_c}{\sqrt{1 + \left(\frac{\mu'}{\mu}\right)^2}}. \quad (14)$$

In the usual practical situation, with $\mu = \mu' \approx 1$, we have $\cos \tilde{\theta} = \frac{1}{\sqrt{2}} \cos \theta_c$. For usual optical media with very weak magnetic properties, one sees that a large index ratio $n/n' \approx \sqrt{\epsilon/\epsilon'}$ does not increase the range of applicability of Dirichlet BC for TM polarization. To give a numerical example, for a weak index mismatch with $\sin \theta_c = 1/2$, giving $\theta_c = 30^\circ$, the crossover angle is $\tilde{\theta} = 52.2^\circ$; in order to reach phase angle $\alpha = 0.9\pi$, quite close to DBC, requires an incident angle $\theta_i = 82.2^\circ$. Even for a larger mismatch $\sin \theta_c = 1/4$, with $\theta_c = 14.5^\circ$, one gets only a slight improvement to $\tilde{\theta} = 46.8^\circ$, and to get to $\alpha = 0.9\pi$ still requires $\theta_i = 81.3^\circ$.

The conclusion is that it makes some reasonable sense to apply NBC to find the limiting conditions for TIR, but, in general, provided the incident angle is sufficiently larger than the crossover angle $\tilde{\theta}$, an approximate description of the fields on the incident side should be possible using DBC. The application of DBC to this problem improves with higher index mismatch, but not as strongly as one would hope, because the phase angle does not depend on the dielectric permittivities for this polarization.

TE polarization: The discussion is similar, but now the magnetic field \vec{B} is polarized in the \hat{z} direction everywhere, and controls the other fields, according to relations $\vec{B} = \sqrt{\epsilon\mu} \hat{k} \times \vec{E}$ for each plane wave, and amplitude relations $B = \sqrt{\epsilon\mu} E$. Taking incident wave $\vec{B}_i = B_i^0 \hat{z} e^{i(k_x x + k_y y)}$, with electric field amplitude $E_i^0 = B_i^0 / \sqrt{\epsilon\mu}$, there is a reflected wave $\vec{B}_r = B_r^0 \hat{z} e^{i(k_x x - k_y y)}$, with electric field amplitude $E_r^0 = B_r^0 / \sqrt{\epsilon\mu}$. Now the amplitude ratio $E_r^0/E_i^0 = e^{-i\alpha}$ is described by the different Fresnel formula:

$$e^{-i\alpha} = \frac{\sqrt{\frac{\epsilon'}{\mu'}} \cos \theta_i - \sqrt{\frac{\epsilon}{\mu}} \cos \theta'}{\sqrt{\frac{\epsilon'}{\mu'}} \cos \theta_i + \sqrt{\frac{\epsilon}{\mu}} \cos \theta'} \quad (15)$$

Clearly, the same amplitude ratio also applies to B_r^0/B_i^0 . The phase difference between the incident and reflected

waves can be expressed as

$$\tan \frac{\alpha}{2} = \frac{\epsilon}{\epsilon'} \sqrt{\frac{\cos^2 \theta_c}{\cos^2 \theta_i} - 1}. \quad (16)$$

The linear combination of incident and reflected magnetic waves in medium n is $\vec{B} = \vec{B}_i + \vec{B}_r = B_z \hat{z}$, and mirrors the behavior of \vec{E} for the TM problem, having the spatial variation approaching the boundary,

$$B_z = B_i + B_r = 2B_i^0 e^{-i\frac{\alpha}{2}} e^{ik_x x} \cos\left(k_y y + \frac{\alpha}{2}\right) \quad (17)$$

The associated evanescent wave in medium n' is

$$B'_z = 2B_i^0 e^{-i\frac{\alpha}{2}} e^{ik_x x} e^{-k' \gamma y}. \quad (18)$$

Clearly, the behavior of B_z near the boundary for TE polarization is the same as that for E_z near the boundary for TM polarization. It means that provided the incident angle is far enough beyond the critical angle, one should also apply DBC for TE fields; NBC would only be reasonable just beyond the TIR threshold. However, due to the presence of the permittivity ratio in (16), a large index mismatch *does* enhance the applicability of DBC for TE polarization. The crossover incident angle $\tilde{\theta}$ at which $\tan \frac{\alpha}{2} = 1$ is now

$$\cos \tilde{\theta} = \frac{\cos \theta_c}{\sqrt{1 + (\frac{\epsilon'}{\epsilon})^2}} \approx \frac{\cos \theta_c}{\sqrt{1 + (\frac{n'}{n})^4}}, \quad (19)$$

where the latter expression applies when $\mu \approx \mu'$. For some numerical examples, now the modest index mismatch with $\sin \theta_c = 1/2$ and $\theta_c = 30^\circ$ leads to a very nearby crossover angle $\tilde{\theta} = 32.8^\circ$, meaning that the strong TIR regime and region of adequate applicability of DBC is very wide. For larger mismatch $\sin \theta_c = 1/4$ with $\theta_c = 14.5^\circ$, the DBC regime is even closer to θ_c , beginning around $\tilde{\theta} = 14.9^\circ$. Thus, application of Dirichlet BC to finding the 2D resonant modes for a cavity with TE field polarization should be very acceptable, even more so than for TM polarization, except when the mode has plane wave components extremely close to their TIR threshold.

Within the limitations indicated in the above analysis, we continue by discussing the modes in a 2D equilateral triangle, under the assumption of DBC for either the TM or TE polarizations.

B. Exact modes for an equilateral triangle with DBC

The triangular cross section offers an opportunity for exact solutions to the 2D Helmholtz equation. This problem has been solved analytically[12, 13, 14, 15] for both DBC and NBC in several contexts, including quantum billiards problems,[17, 19, 20, 21] quantum dots,[16]

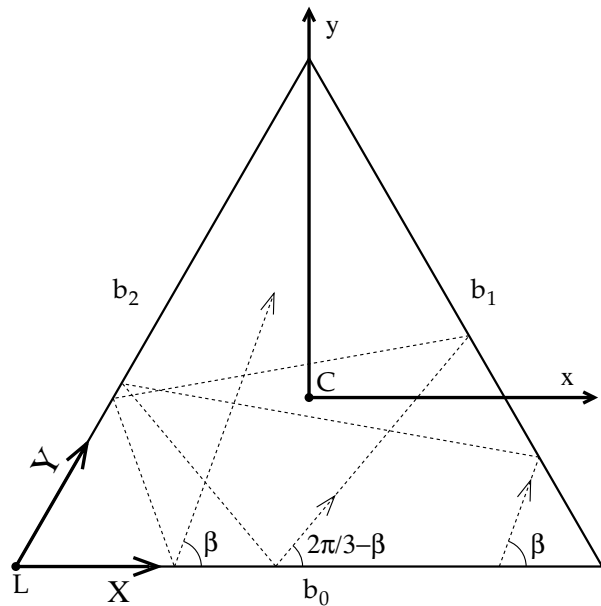


FIG. 1: Description of the coordinates for a 2D triangular cavity of edge a . The geometrical center at C , the origin of the xy -coordinates, is a distance $\frac{a}{2\sqrt{3}}$ above the lower (b_0) edge. The lower left corner at L is the origin of the skew XY -coordinates. The dashed line demonstrates the reflections of a ray originating at angle $\beta = 70^\circ$ to the lower edge, requiring two complete circuits to return to the same angle.

and lasing modes in resonators and mirrored dielectric cavities.[2, 22] In particular, it is interesting to note that only the triangles with angle sets $\pi(\frac{1}{3}, \frac{1}{3}, \frac{1}{3})$, $\pi(\frac{1}{2}, \frac{1}{4}, \frac{1}{4})$, and $\pi(\frac{1}{2}, \frac{1}{3}, \frac{1}{6})$ are classically integrable[20] and have simple closed form wavefunction solutions derived in various ways,[13, 14, 21] following the first solution for triangular elastic membranes by Lamé.[12] Here we use the equilateral triangle of edge length a for its interesting symmetries and resulting simplifications.

Coordinates are used where the origin is placed at the geometrical center of the triangle, and the lower edge is parallel to the x -axis, as shown in Fig. 1. The notation b_0 , b_1 , and b_2 is used to denote the lower, upper right, and upper left boundaries, respectively. This discussion concerns DBC.

Following Chang *et al.*,[2] some comments can be made on the sequence of reflections a plane wave trapped in the cavity makes, but with a slightly different physical interpretation. A plane wave leaving the lower face (b_0) at angle β to the x -axis sequentially undergoes reflections at the other two faces, generating plane waves at angles $240^\circ - \beta$, $\beta - 120^\circ$, relative to the x -axis. Finally, when reflected again off the lower face, it comes out at $120^\circ - \beta$, which does not match the original wave unless $\beta = 60^\circ$. However, when allowed to propagate *again* around the triangle, the sequence of angles is $120^\circ + \beta$, $-\beta$, which then comes out at $+\beta$ after the reflection off the lower face. So the wave closes on itself after two full revolu-

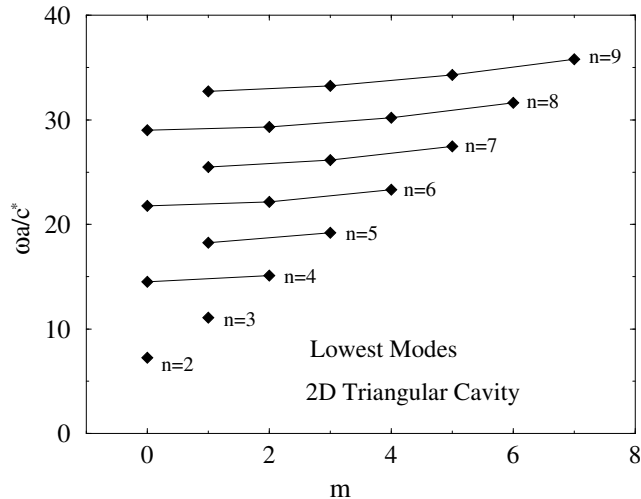


FIG. 2: Scaled frequencies of some of the lowest possible modes in a 2D triangular system, as a function of quantum index m , for indicated $n > m$. Indices n and m must be integers of equal parity. c^* is the light speed in the medium.

tions, no matter what the initial angle. As an example, the sequence of reflections starting with $\beta = 70^\circ$ from boundary b_0 are shown in Fig. 1. In general, any original wave simply generates a set of six symmetry related waves rotated by $\pm 120^\circ$ and inversions through the y -axis.

These considerations show that the general solution is a superposition of six plane waves, which can be obtained by 120-degree rotations of one partially standing wave. Consider initially a wavevector with xy Cartesian components, $\vec{k} = (k_1, k_2)$, and defined basic vectors $\vec{k}_1 = k_1 \hat{x}$, $\vec{k}_2 = k_2 \hat{y}$, producing a wavefunction written as

$$\psi_0 = e^{i\vec{k}_1 \cdot \vec{r}} \sin \left[\vec{k}_2 \cdot \vec{r} + \frac{k_2 a}{2\sqrt{3}} \right] \quad (20)$$

This is a combination of plane waves at two angles β and $-\beta$ to the x -axis, where $\tan \beta = k_2/k_1$, and the combination goes to zero on boundary b_0 , where $y = -\frac{a}{2\sqrt{3}}$; thus it is like a standing wave. By assumption, we need $k_2 \neq 0$ to have a nonzero wavefunction. As discussed above, when reflected off the triangle faces b_1 and b_2 , this simply produces rotations of $\pm 120^\circ$. If R is an operator that rotates vectors through $+120^\circ$, the additional waves being generated are

$$\psi_1 = e^{i(R\vec{k}_1) \cdot \vec{r}} \sin \left[(R\vec{k}_2) \cdot \vec{r} + \frac{k_2 a}{2\sqrt{3}} \right] \quad (21)$$

$$\psi_2 = e^{i(R^2\vec{k}_1) \cdot \vec{r}} \sin \left[(R^2\vec{k}_2) \cdot \vec{r} + \frac{k_2 a}{2\sqrt{3}} \right] \quad (22)$$

where the rotated vectors are

$$R\vec{k}_1 = k_1 \left(-\frac{1}{2}\hat{x} + \frac{\sqrt{3}}{2}\hat{y} \right) \\ R^2\vec{k}_1 = k_1 \left(-\frac{1}{2}\hat{x} - \frac{\sqrt{3}}{2}\hat{y} \right) \quad (23)$$

$$R\vec{k}_2 = k_2 \left(-\frac{\sqrt{3}}{2}\hat{x} - \frac{1}{2}\hat{y} \right) \\ R^2\vec{k}_2 = k_2 \left(\frac{\sqrt{3}}{2}\hat{x} - \frac{1}{2}\hat{y} \right) \quad (24)$$

By design, these rotated waves satisfy the boundary conditions, $\psi_1(b_1) = 0$ and $\psi_2(b_2) = 0$.

In order to determine the allowed (k_1, k_2) , one needs to impose DBC on all three boundaries, for a linear combination with unknown coefficients $\mathcal{A}_0, \mathcal{A}_1, \mathcal{A}_2$,

$$\psi = \mathcal{A}_0\psi_0 + \mathcal{A}_1\psi_1 + \mathcal{A}_2\psi_2. \quad (25)$$

Imposing DBC on all boundaries determines the allowed wavevector components as

$$k_1 = \frac{2\pi}{3a}m, \quad m = 0, 1, 2, \dots \quad (26)$$

$$k_2 = \frac{2\pi}{3a}\sqrt{3}n, \quad n = 1, 2, 3, \dots \quad (27)$$

Furthermore, the parity constraint $e^{i\pi m} = e^{i\pi n}$ appears; that is, n and m are either both odd or both even.

The resulting xy frequencies are given by

$$\omega = c^* \sqrt{k_1^2 + k_2^2} = \frac{c}{\sqrt{\epsilon\mu}} \frac{2\pi}{3a} \sqrt{m^2 + 3n^2} \quad (28)$$

The mode wavefunctions are described completely using the amplitude relationships that result:

$$\mathcal{A}_1 = \mathcal{A}_0 e^{i\frac{2\pi}{3}m}, \quad \mathcal{A}_2 = \mathcal{A}_0 e^{-i\frac{2\pi}{3}m}. \quad (29)$$

Therefore, solutions are specified by a choice of integers m and n and the phase of the complex constant \mathcal{A}_0 . In Fig. 2 the frequencies of the lowest modes are presented, scaled with the speed of light in the medium, c^* , and arranged as families for each value of the quantum number n . This solution is represented in the physically motivated form described by Chang *et al.*,[2] and is entirely equivalent to the first solution given by Lamé'[12] and revisited by various authors.[15]

The solutions obtained have obvious symmetry properties. We can get all the possible eigenfrequencies by applying the restrictions, $0 \leq m < n$. Choices with $m \geq n$ or $m < 0$ also give allowed frequencies, however, these only correspond to other \vec{k} rotated by $\pm 120^\circ$

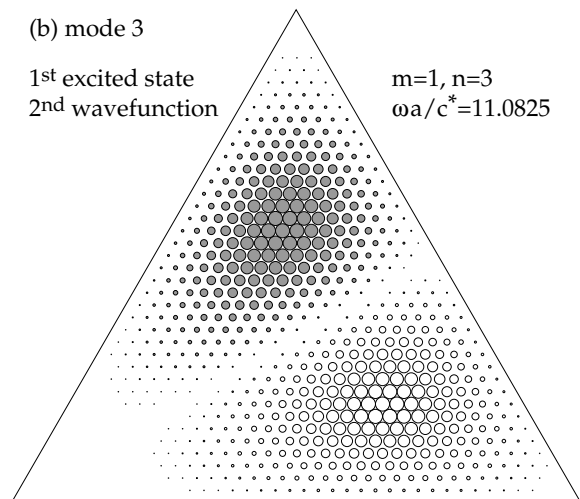
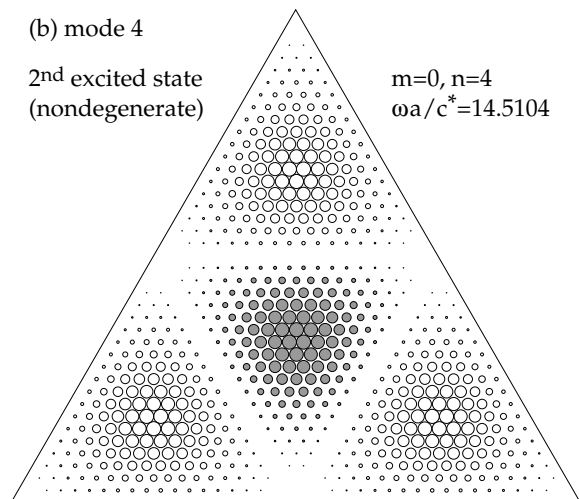
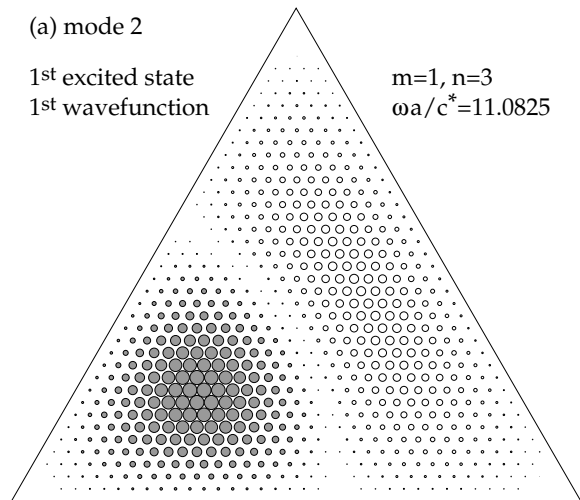
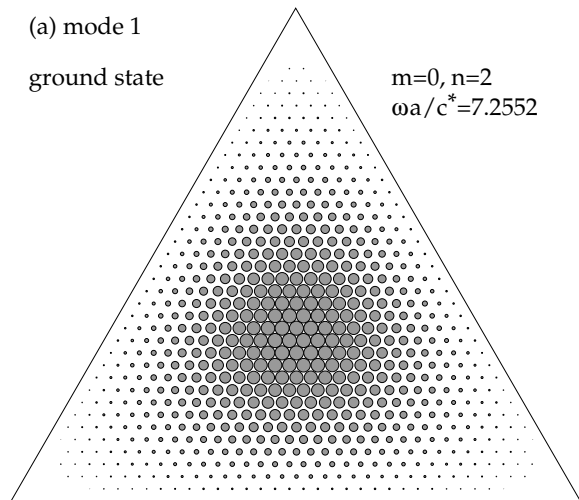


FIG. 3: Wavefunctions of the two lowest modes with $m = 0$ in a 2D triangular system: the ground state (a), with $n = 2$, and the third excited state (b), with $n = 4$, at double the frequency of the ground state. Solid/partial shadings represent positive/negative wavefunction values, whose magnitudes correspond to the radii of the symbols. A grid with $N = 40$ was only used to present the diagrams. Grid sites without symbols have $|\psi| < 0.02|\psi_{\max}|$.

from some original \vec{k} defined with $0 \leq m < n$. For instance, having found $\vec{k} = (k_1, k_2) = \frac{2\pi}{3a}(m, \sqrt{3}n)$, values of $\vec{k}' = (k'_1, k'_2) = \frac{2\pi}{3a}(m', \sqrt{3}n')$ corresponding to $\pm 120^\circ$ rotations result from

$$\begin{aligned} k'_1 &= k_1 \cos 120^\circ \mp k_2 \sin 120^\circ \\ k'_2 &= \pm k_1 \sin 120^\circ + k_2 \cos 120^\circ \end{aligned} \quad (30)$$

FIG. 4: Wavefunctions of the doubly degenerate first excited state in a 2D triangular system. Two orthogonal sub-states corresponding to different choices of the phase of ψ are presented in (a) and (b).

which implies transformation to the new mode indexes,

$$\begin{aligned} m' &= -\frac{1}{2}m \mp \frac{3}{2}n \\ n' &= \pm \frac{1}{2}m - \frac{1}{2}n. \end{aligned} \quad (31)$$

As specific examples, the choice $(m, n) = (1, 3)$ gives one mode, which after rotations by $\pm 120^\circ$ could also be described by the integers $(m, n) = (4, 2)$ or by $(m, n) = (5, 1)$. Note, however, this represents only one mode, with different choices of the reference edge or triangle base. We should also note, any mode with $m \neq 0$ is doubly degenerate; the change $m \rightarrow -m$ gives an independent mode with the same frequency, which rotates in the opposite sense around the triangle. A real representation of the degenerate pairs comes from taking the real

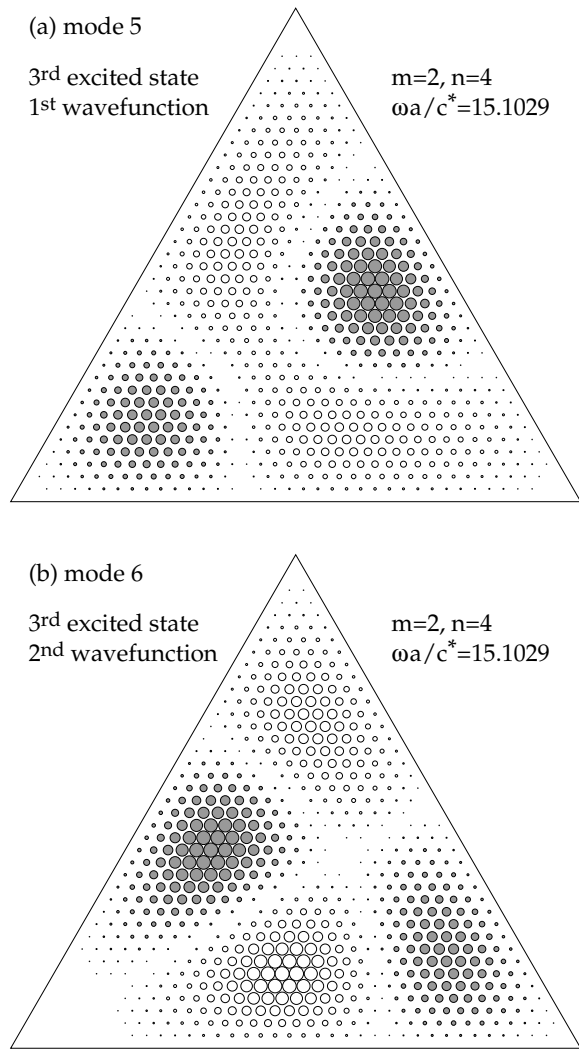


FIG. 5: Wavefunctions of the doubly degenerate third excited state in a 2D triangular system. Two orthogonal sub-states corresponding to different choices of the phase of ψ are presented in (a) and (b).

and imaginary parts of ψ to form two independent wavefunctions. Different values of the complex constant \mathcal{A}_0 will produce other choices of the two independent wavefunctions. For $m = 0$, the wavefunction ψ can be made pure real; the modes are non-degenerate and n must be even, since m and n must be of equal parity.

The ground state (Fig. 3a) has $(m, n) = (0, 2)$ and corresponding xy frequency, $\omega = \frac{c}{\sqrt{\epsilon\mu}} \frac{4\pi}{\sqrt{3}a}$. This corresponds to a wavelength of $\lambda = \frac{2\pi}{k} = \frac{\sqrt{3}a}{2}$, which is equal to the height of the triangle. Naively, one might have expected that a half-wavelength of the lowest mode could have fit across the triangle, as would occur in simple rectangular or one-dimensional geometry. Apparently, that choice would not have the ability to fully satisfy DBC on all three surfaces.

The wavefunctions of the lowest modes with $m = 0$ are displayed in Fig. 3. All the modes with $m = 0$ have this typical triangular shape, periodically patterned over the entire system. Wavefunctions of the first two excited states are presented in Figs. 4 and 5. Each of these states, having nonzero m , is doubly degenerate, therefore, there is some arbitrariness in the wavefunction pictures. Two degenerate wavefunctions were obtained from the real and imaginary parts of ψ in Eq. (25); an equivalent degenerate pair can be obtained by changing the complex constant \mathcal{A}_0 . The degenerate pairs can be shown to be orthogonal in the usual sense. Wavefunctions for the sequence of many of the other lowest modes are displayed at www.phys.ksu.edu/~wysin/. The modes described here are the complete set of allowed modes for the triangular geometry.

C. Equilateral triangle with NBC

Although we do not apply these in this work, it is interesting to note the minor differences in the solutions when the triangle is solved with Neumann BC.[15] As far as the changes in the wavefunctions, NBC simply requires the *sine* functions in the expressions for ψ_0 , ψ_1 , and ψ_2 , Eqs. (20), (21), (22), to be replaced by *cosine* functions. The expressions (26) and (27) for the allowed wavevectors are still valid, except that the restriction $m < n$ should be changed to $m \leq n$. So the spectrum is expanded slightly, there is an entire set of nondegenerate lower modes with $m = n$ (alternatively with rotated indexes $(m, 0)$); the NBC ground state is lower than the DBC ground state.

D. 3D prisms

For a 3D triangular-based prism of height h , and base edge a , the solutions to the wave equation can be written as products of an xy -dependent part ψ_{xy} and a part ψ_z depending only on the vertical coordinate z . The corresponding k and k_z have already been discussed above. Solutions can be found combining k and ψ_{xy} from the 2D solutions with the k_z and ψ_z discussed above. This approach would assume DBC over the all surfaces of the cavity. While the physical situation would not exactly satisfy the requirements for classification of modes in TM and TE polarizations, the error in this assumption should be least at small k_z . Thus, it could give some rough idea about the modification of the confined modes due to the finite vertical height of the cavity.

III. TIR CONFINEMENT AND THE RESONANT MODE SPECTRUM

Knowing the eigenmodes of the cavity, various questions can be addressed and answered based on the structure of the wavefunctions. The primary question is:

which modes are confined by TIR (or resonant) when the previously assumed Dirichlet boundary conditions are replaced by an index mismatch at the boundary? As seen below, some states can never be TIR confined. States which have the possibility for confinement will be referred to as TIR states. Related to this is to estimate a decay time for any of the TIR modes.

As suggested in the Introduction, the mode confinement can be determined approximately by identifying those modes which completely satisfy the elementary requirements for total internal reflection. We assume that outside the system boundary a different refractive material with relative permeability μ' and permittivity ϵ' (which could be vacuum for greatest simplicity) and index $n' = \sqrt{\epsilon'\mu'}$, rather than a conducting boundary. The wavefunction analysis above describes a mode as a superposition of plane waves with the specified (full 3D) wavevectors \vec{K} . Each plane wave component can be analyzed to see whether it undergoes TIR at all system boundaries on which it is incident. If all the plane wave components of a mode satisfy the TIR requirements, then the mode is confined; it should correspond to a resonance of the optical cavity. If any of the plane wave components do not satisfy TIR, the fields of the mode will quickly leak out of the cavity and there should be no resonance at that mode's frequency (also, without TIR, the assumption of DBC is completely invalidated). These results clearly depend on the index ratio from inside to outside the cavity, denoted as

$$N = \frac{n}{n'} = \frac{\sqrt{\epsilon\mu}}{\sqrt{\epsilon'\mu'}} \quad (32)$$

A plane wave within the cavity with (3D) wavevector \vec{K}_i has an incident angle on one of the boundaries expressed as

$$\sin \theta_i = \frac{K_{i\parallel}}{K_i}, \quad (33)$$

where \parallel indicates the component parallel to the boundary. TIR will take place for this wave provided

$$\sin \theta_i > \sin \theta_c = \frac{1}{N}. \quad (34)$$

For 2D geometry, Eqs. (34) is applied directly to 2D wavevectors, $\vec{K}_i = \vec{k}_i$: one just needs to identify the parallel component of \vec{k}_i relative to a boundary, for each for each plane wave present in ψ , Eq. (25). The main difficulty is to satisfy TIR on all boundaries on which that component is incident.

For 3D prismatic geometry, the wavevector \vec{K}_i includes a z -component. The net parallel component needed in (34) can include planar (xy) and vertical (z) contributions. The addition of a z -component will have the tendency to raise the energy of any mode, and the net wavevector magnitude, thereby improving the possibility for mode confinement.

A. Confinement in 2D triangular systems

For both the TM and TE 2D modes of an equilateral triangle, we can use the exact solutions in Sec. IIB to investigate whether these can be confined by TIR. Due to the threefold rotational symmetry through angles of 0° , 120° and -120° , the TIR condition need only be applied on one of the boundaries, say, the lower boundary b_0 , parallel to the x -axis. The first wave ψ_0 is composed of two traveling waves, one incident on b_0 and one reflected from b_0 ; both have wavevectors whose x -component is $k_1 = \frac{2\pi}{3a}m$, where $m = 0, 1, 2, \dots$. The other rotated waves ψ_1 and ψ_2 are composed from traveling waves whose wavevectors have x -components of magnitudes $\frac{1}{2}(\sqrt{3}k_2 \pm k_1)$, where $k_2 = \frac{2\pi}{3a}\sqrt{3}n$ with $n = 1, 2, 3, \dots$. For the allowed modes, $m < n$, or $k_1 < k_2$, which shows that

$$k_1 < \frac{1}{2}(\sqrt{3}k_2 - k_1) \leq \frac{1}{2}(\sqrt{3}k_2 + k_1). \quad (35)$$

The x -component of the ψ_0 wave is always the smallest; this wave has the smallest angle of incidence on b_0 , so if it undergoes TIR then so do ψ_1 and ψ_2 , and the mode is confined. As k_1 is the component parallel to boundary b_0 (i.e., $k_{i\parallel}$), the condition for TIR confinement of the mode is

$$\sin \theta_i = \frac{k_1}{\sqrt{k_1^2 + k_2^2}} > \sin \theta_c = \frac{1}{N}, \quad (36)$$

or equivalently in terms of quantum numbers m and n ,

$$\frac{m}{n} > \sqrt{\frac{3}{N^2 - 1}}. \quad (37)$$

This relation contains some interesting features. First, since all modes have $m < n$, the LHS is always less than 1, and confinement of modes can only occur for adequately large refractive index ratio, $N > 2$. For $N < 2$ all modes will leak out of the cavity; they cannot be stably maintained by TIR. Secondly, for any particular value $N > 2$, relation (37) determines a critical m/n ratio; modes whose m/n ratio is below the critical value will not be stable. As m/n relates to the geometrical structure of the mode wavefunction, there is a strong relation between the confined mode structures and the refractive index. An alternative way to look at this, is that each particular mode will be confined only if N is greater than a specific critical value determined by the m/n ratio for that mode:

$$N > N_c = \sqrt{3\frac{n^2}{m^2} + 1}. \quad (38)$$

The relation shows that generally speaking, modes with smaller n/m are most easily confined; stated otherwise, the modes where m is closest to n are the ones most readily confined. On the other hand, all modes with $m = 0$ leak out, because these have wave components with a vanishing angle of incidence on the boundaries.

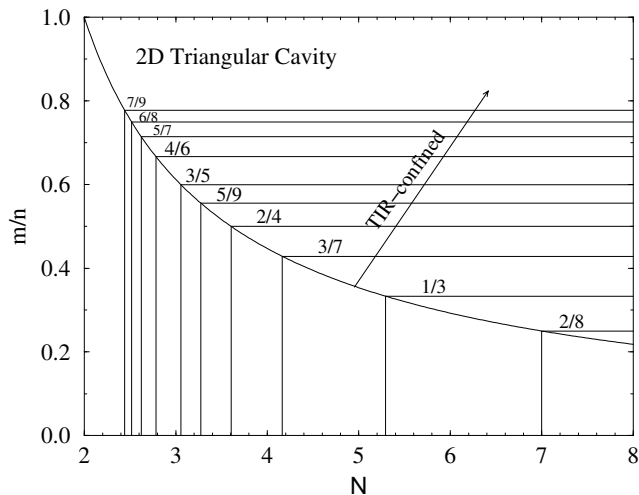


FIG. 6: TIR mode confinement limits (index ratio $N = \sqrt{\epsilon\mu/\epsilon'\mu'}$) for 2D triangular cavities. Modes are confined where the m/n ratios (as indicated) lie above the solid curve, corresponding to TIR on all boundaries [relation (37)]. Intersections on the N -axis give the critical index ratios for each mode.

Fig. 6 is a kind of phase diagram for mode confinement by TIR. Some of the modes' m/n ratios are plotted vs. refractive index ratio N , together with relation (37). A particular mode is confined only if its m/n value falls above the critical curve. In this way one can easily see the critical refractive indexes for each mode. As mentioned above, modes where m is close to n require the smallest refractive index values for confinement.

One more application of these results is shown in Fig. 7, where the frequency of the lowest confined mode is plotted versus $\sqrt{\epsilon\mu}$, with vacuum outside the cavity ($\epsilon'\mu' = 1$). The quantum numbers (m, n) for the lowest confined mode are indicated in each curve segment. The two different curves correspond to plotting $\omega a/c$ (dashed) and frequency scaled with refractive index, $(\omega a/c)\sqrt{\epsilon\mu}$ (solid). Of course, as $\sqrt{\epsilon\mu}$ approaches the value 2, the lowest frequency becomes large and the minimizing mode has m very close to n , with both large. At the opposite limit of large values of $\sqrt{\epsilon\mu}$, the lowest frequency becomes small, and the mode (1, 3) is always the lowest frequency mode that is confined for any $\sqrt{\epsilon\mu} > 5.29$. The graph only shows the minimum confined frequency at the intermediate values of refractive index $\sqrt{\epsilon\mu}$.

B. Confinement in triangular based prisms

We consider a vertical prism of height h with a triangular base of edge a . With perfectly reflecting end mirrors at $z = 0$ and $z = h$ the allowed longitudinal wavevectors would be $k_z = l\pi/h$, where l is an integer. For a plane wave component with 2D wavevector \vec{k}_i , the net

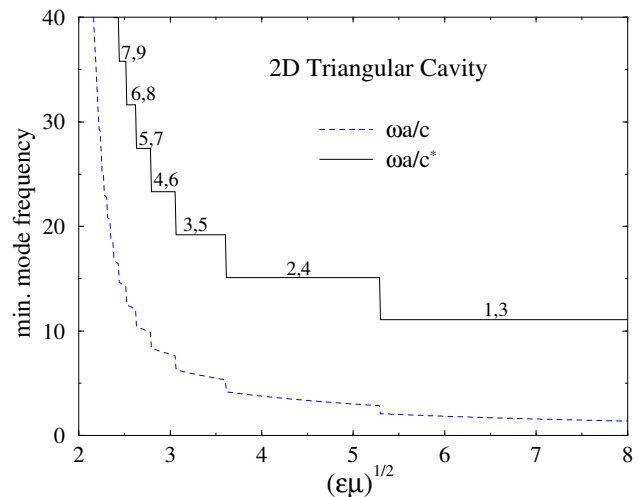


FIG. 7: Frequency of the lowest confined mode for a 2D triangular system surrounded by vacuum, as a function of the refractive index. Pairs (m, n) indicate some of the modes' quantum numbers. No modes are confined for $\sqrt{\epsilon\mu} \leq 2$.

3D wavevector magnitude within the cavity is

$$K_i = \sqrt{k_i^2 + k_z^2}. \quad (39)$$

This increases the incident angles on the walls of the cavity: the presence of nonzero k_z should enhance the possibility for confinement, compared to the purely 2D system.

At the lower and upper ends of the prism, the parallel wavevector component of any of the plane waves present is the full 2D \vec{k}_i , which can be expressed as

$$K_{i||}^{(\text{ends})} = |\vec{k}_i| = \sqrt{k_1^2 + k_2^2} = \frac{2\pi}{3a} \sqrt{m^2 + 3n^2}. \quad (40)$$

Finding the incident angle by (33) and Snell's Law (34), this implies a critical index ratio needed for TIR confinement by the cavity ends,

$$N_c^{(\text{ends})} = \frac{1}{\sin \theta_i} = \sqrt{1 + \left(\frac{3}{2\pi}\right)^2 \frac{(k_z a)^2}{m^2 + 3n^2}}. \quad (41)$$

On the vertical walls of the prism, the parallel wavevector component is a combination of k_z and the 2D $k_{i||}$. If TIR occurs on one wall then by symmetry it will take place on all the walls. Considering the b_0 wall, the ψ_0 wave has the largest incident angle as in the 2D problem, and both k_1 and k_z determine its parallel wavevector component,

$$K_{i||}^{(\text{walls})} = \sqrt{k_1^2 + k_z^2} = \sqrt{\left(\frac{2\pi}{3a}\right)^2 m^2 + k_z^2}. \quad (42)$$

Then this determines the critical index ratio needed for TIR by the cavity walls,

$$N_c^{(\text{walls})} = \frac{1}{\sin \theta_i} = \sqrt{1 + \frac{3n^2}{m^2 + \left(\frac{3}{2\pi}\right)^2 (k_z a)^2}}. \quad (43)$$

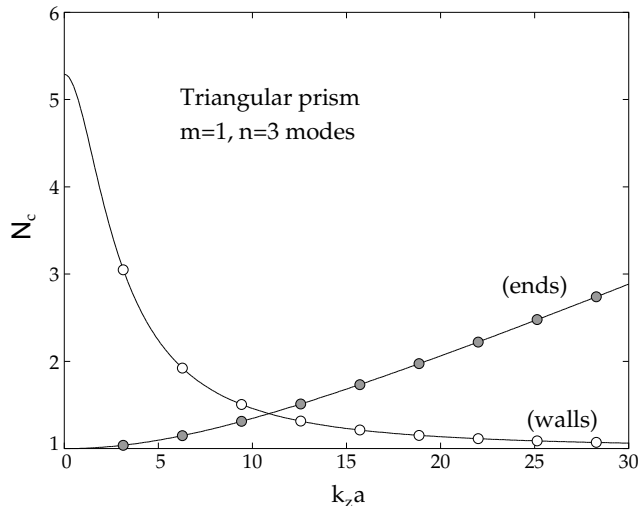


FIG. 8: Triangular prism critical index ratios for TIR from the walls (open symbols) and ends (solid symbols) of the cavity, for the modes with 2D quantum indexes $m = 1$, $n = 3$, and longitudinal wavevector k_z . The symbols show the allowed $k_z a$ values $l\pi a/h$ when $h = a$.

For TIR mode confinement, the actual index ratio N must be greater than both $N_c^{(\text{ends})}$ and $N_c^{(\text{walls})}$.

Some results are shown in Fig. 8 for the $m = 1$, $n = 3$ modes as a function of k_z . The symbols indicate the allowed k_z values for the prism height equal to the base edge, $h = a$. The limiting 2D critical ratio is seen at the point $k_z a = 0$. The critical index ratio is lowered from the 2D value $N_c \approx 5.29$, down to values as low as $N_c \approx 1.40$ for $k_z a \approx 11$. A more significant reduction in N_c occurs for the ground state, $m = 0$, $n = 2$, Fig. 9. It is not possible to confine this mode in 2D; whereas, it has $N_c \approx 1.41$ for $k_z a \approx 7.25$. Similar significant critical index ratio reductions occur for all the modes tested.

One sees that $N_c^{(\text{walls})}$ and $N_c^{(\text{ends})}$ always cross at some intermediate k_z , where they produce the smallest index ratio $N_c^{(\text{min})}$ needed for TIR. Setting them equal, we find

$$N_c^{(\text{min})} = \sqrt{1 + \left(1 + \frac{m^2}{3n^2}\right)^{-1}}, \quad (44)$$

which occurs at

$$k_z^* = \left(\frac{2\pi}{3a}\right) \sqrt{3n} = k_2. \quad (45)$$

It is a rather intriguing result; choosing h/a such that a mode will occur at this k_z will be the optimum choice for having the mode confined most easily by TIR. This could be useful for control over selection of desired modes in a cavity.

Cautionary comments are in order. The above discussion applies exactly only to a scalar wave. For electromagnetic waves, it applies to either the TM or TE

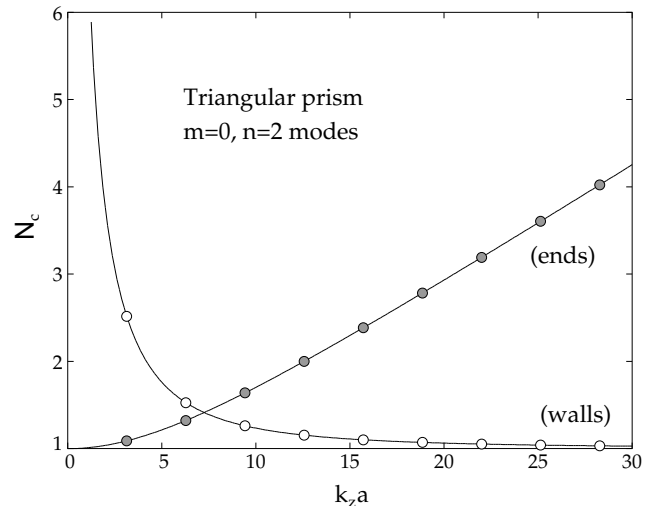


FIG. 9: Triangular prism critical index ratios as explained in Fig. 8 for the modes with 2D quantum indexes $m = 0$, $n = 2$ (2D ground state).

polarizations in an approximate sense for quasi-2D EM modes, requiring small longitudinal wavevector $k_z a < 1$. The greatest enhancements in TIR were found to occur at values $k_z a > 1$, primarily because a reasonably large k_z is needed in order to satisfy the TIR requirements at the ends. The presence of significant k_z values, however, will lead to a mixing of the TM and TE polarizations, making this calculation invalid. Then, for practical purposes, the calculation is mostly interesting for how it indicates the improvement in TIR confinement expected mainly on the 2D walls of the cavity, at small k_z .

IV. TIR MODE LIFETIMES

For the 2D solutions ($k_z = 0$), it is interesting to estimate the lifetimes of the TIR-confined modes, contrasting the results for TM and TE polarizations. When all of the plane wave components in ψ satisfy the TIR conditions, there is still the possibility for the cavity fields to decay in time. Clearly, we have only an approximate solution, since DBC is not exactly the correct boundary condition. The effect this causes is difficult to estimate. Another source of decay are diffractive effects: the finite length of the triangle edge and the presence of sharp corners is likely to have special influence on the TIR that is difficult to predict. One feature, however, which can be considered as due to diffraction, is the leakage of *boundary waves* at the corners of the triangle.[23] Under conditions of TIR, an evanescent wave exists within the exterior medium, decaying exponentially into that medium, and moving parallel to the cavity surface. When it encounters the corner of that edge, a sharp discontinuity in the surface, it can be expected to constitute power radiated from the cavity. Here we consider the mode lifetime

estimates based solely on the losses due to these boundary waves.

Based on the ratio of the total energy U stored in the cavity fields, compared to the total power P emitted by the boundary waves from all the corners, an upper limit of the mode lifetime can be estimated as

$$\tau = \frac{U}{P}. \quad (46)$$

The calculations of U and P have slight differences for TM versus TE polarization. Therefore, there is no reason to expect these lifetimes to be the same.

Cavity energy: For both polarizations, we use the wavefunction ψ reviewed in Sec. II B, which can be expressed more succinctly as

$$\begin{aligned} \psi = \mathcal{A}_0 & \left\{ e^{ik_1 x} \sin \left[k_2 \left(y + \frac{a}{2\sqrt{3}} \right) \right] \right. \\ & + e^{ik_1 \left(-\frac{1}{2}x + \frac{\sqrt{3}}{2}y + a \right)} \sin \left[k_2 \left(-\frac{\sqrt{3}}{2}x - \frac{1}{2}y + \frac{a}{2\sqrt{3}} \right) \right] \\ & \left. + e^{ik_1 \left(-\frac{1}{2}x - \frac{\sqrt{3}}{2}y - a \right)} \sin \left[k_2 \left(\frac{\sqrt{3}}{2}x - \frac{1}{2}y + \frac{a}{2\sqrt{3}} \right) \right] \right\} \end{aligned} \quad (47)$$

The total energy of the fields within the cavity of height h can be written as

$$U = \int h \, dx dy \frac{\epsilon |\vec{E}|^2}{8\pi} = \int h \, dx dy \frac{|\vec{B}|^2}{8\pi\mu}; \quad (48)$$

the first form is convenient for TM modes ($|\vec{E}|^2 = |\psi|^2$), the second is convenient for TE modes ($|\vec{B}|^2 = |\psi|^2$). So both calculations require the normalization integral of ψ . This integral can be simplified by a transformation to a skew coordinate system whose axes are aligned to two edges of the triangle as shown in Fig. 1. Placing the origin of the new coordinates (X, Y) at the lower left corner of the triangle, with X increasing from 0 to a along edge b_0 , and Y increasing from 0 to a along edge b_2 , the definition of the new coordinates results from

$$\begin{aligned} X + Y \cos 60^\circ &= x + \frac{a}{2}, \\ Y \sin 60^\circ &= y + \frac{a}{2\sqrt{3}}. \end{aligned} \quad (49)$$

The numbers $(\frac{a}{2}, \frac{a}{2\sqrt{3}})$ are simply the displacement of the origin (vector from triangle corner L to center C). The wavefunction is now expressed as

$$\begin{aligned} \psi = \mathcal{A}_0 & \left\{ e^{ik_1 \left(X + \frac{1}{2}Y - \frac{a}{2} \right)} \sin \left[\frac{\sqrt{3}}{2} k_2 Y \right] \right. \\ & + e^{ik_1 \left(-\frac{1}{2}X + \frac{1}{2}Y + a \right)} \sin \left[\frac{\sqrt{3}}{2} k_2 \left(-X - Y + a \right) \right] \\ & \left. + e^{ik_1 \left(-\frac{1}{2}X - Y - \frac{a}{2} \right)} \sin \left[\frac{\sqrt{3}}{2} k_2 X \right] \right\}. \end{aligned} \quad (50)$$

In this form, it is more obvious that each term goes to zero on one of the boundaries, $X = 0$ (b_2), $Y = 0$ (b_0),

or $X + Y = a$ (b_1). Using the periodicity of ψ , the integration over the triangular area is effected by

$$\int dx dy = \frac{1}{2} \int_0^a dX \int_0^a dY |J| \quad (51)$$

where the Jacobian is $|J| = \frac{\sqrt{3}}{2}$ and the factor of $\frac{1}{2}$ cancels integrating over two triangles. The absolute square of ψ involves three direct terms (squared sines involving only k_2) and six cross terms from Eq. (50). It is possible to show that the cross terms integrated over the triangular area all are zero, due to the special choices of allowed k_1 and k_2 given by (26) and (27). The remaining nonzero parts result in

$$\int dx dy |\psi|^2 = \frac{3\sqrt{3}}{8} a^2 |\mathcal{A}_0|^2. \quad (52)$$

Boundary wave power: The symmetry of the wavefunction causes the boundary wave power out of each edge to be the same, therefore, we calculate that occurring in edge b_0 (at $y = 0$) and multiply by three for the total power. This calculation follows that presented by Wiersig[23] for resonant fields in a regular polygon.

Looking at the wavefunction (47), one can see that there are three distinct plane waves *incident* on b_0 . First is the wave with the smallest angle of incidence, resulting from the first term in (47),

$$\psi_0^- = \frac{-\mathcal{A}_0}{2i} e^{\frac{-ik_2 a}{2\sqrt{3}}} e^{i(k_1 x - k_2 y)}. \quad (53)$$

Using the allowed values for k_1 and k_2 , the angle of incidence is seen to be

$$\sin \theta_0^- = \frac{m}{\sqrt{m^2 + 3n^2}}. \quad (54)$$

Next, there is a wave with the largest magnitude incident angle, due to the second term in (47),

$$\psi_1^+ = \frac{\mathcal{A}_0}{2i} e^{i(k_1 + \frac{k_2}{2\sqrt{3}})a} e^{i[(-\frac{1}{2}k_1 - \frac{\sqrt{3}}{2}k_2)x + (\frac{\sqrt{3}}{2}k_1 - \frac{1}{2}k_2)y]}, \quad (55)$$

whose incident angle is

$$\sin \theta_1^+ = \frac{1}{2} \frac{-m - 3n}{\sqrt{m^2 + 3n^2}}. \quad (56)$$

A negative value of θ_{1+} means the wave is propagating contrary to the $x - axis$. Finally, the last term in (47) leads to a wave with an intermediate incident angle,

$$\psi_2^+ = \frac{\mathcal{A}_0}{2i} e^{i(-k_1 + \frac{k_2}{2\sqrt{3}})a} e^{i[(-\frac{1}{2}k_1 + \frac{\sqrt{3}}{2}k_2)x + (-\frac{\sqrt{3}}{2}k_1 - \frac{1}{2}k_2)y]}, \quad (57)$$

whose incident angle is

$$\sin \theta_2^+ = \frac{1}{2} \frac{-m + 3n}{\sqrt{m^2 + 3n^2}}. \quad (58)$$

The plus/minus superscripts on these waves refer to the positive/negative exponents in the sine functions of Eq. (47).

Now, for each of these incident waves, there is a corresponding evanescent wave propagating along the edge of the cavity; these are assumed to produce emitted power when encountering the triangle corners. The Poynting vector \vec{S}' associated with a single plane evanescent wave along the b_0 boundary is

$$\vec{S}' = \frac{c}{8\pi} \Re(\vec{E}' \times \vec{H}'^*) = \frac{c}{8\pi} \sqrt{\frac{\epsilon'}{\mu'}} |\vec{E}'|^2 \sin \theta' \hat{x} \quad (59)$$

On the other hand, the linear superposition of the three waves $\psi_0^-, \psi_1^+, \psi_2^+$ leads to an interference pattern both within the cavity, and in the evanescent waves and exterior power flow. Careful consideration of a linear combination of two waves shows that, although interference leads to a spatially varying \vec{S}' with components both parallel and perpendicular to the boundary, an integral number of wavelengths of that pattern fits along the edge. Thus, it is clear that the interference effects can be ignored in the calculation of the emitted boundary power. For the total emitted power due to boundary waves, it is sufficient to sum the individual powers for the three independent incident waves.

For **TM polarization**, with $\psi = E_z$, the exterior electric field of a single evanescent wave has only a z -component like that in Eq. (II A). Applying Snell's law, and integrating the Poynting vector from $y = 0$ to $y = \infty$, the power flow along \hat{x} in one boundary wave, on one edge, is

$$P_x = \frac{ch}{4\pi\mu'} \frac{|E_i^0|^2}{\omega/c} \frac{n \sin \theta_i}{\sqrt{(n \sin \theta_i)^2 - (n')^2}} \cos^2 \frac{\alpha}{2} \quad (60)$$

where α is the phase shift given by (11) in Sec. II A. One can see that the boundary wave power has a dependence on $(\sin \theta_i - \sin \theta_c)^{-1/2}$. Although each of the waves $\psi_0^-, \psi_1^+, \psi_2^+$ will produce a boundary wave emission, the wave ψ_0^- has the smallest angle of incidence, and produces by far the largest boundary wave power. This can be seen by examining the expressions for incident angles θ_0^-, θ_1^+ and θ_2^+ , and using the facts that $m < n$ and m, n have the same parity. Therefore a good lifetime estimate can be made using only the power due to ψ_0^- . From the expression (53) for ψ_0^- , the squared magnitude of its electric field is $|E_i^0|^2 = \frac{1}{4} |\mathcal{A}_0|^2$. From expressions (52) and (48), the total TM cavity energy is

$$U_{\text{TM}} = \frac{\epsilon h}{8\pi} \frac{3\sqrt{3}}{8} a^2 |\mathcal{A}_0|^2. \quad (61)$$

The estimate of the lifetime due to boundary wave emission only, from all three edges combined, is $\tau_{\text{TM}} \approx U_{\text{TM}}/3P_x$. It is convenient to express the result in dimensionless form, scaling with the mode frequency,

$$\omega \tau_{\text{TM}} \approx \frac{\sqrt{3}}{4} \left(\frac{\omega a}{c^*} \right)^2 \frac{\sqrt{1 - (\sin \theta_c / \sin \theta_0^-)^2}}{\cos^2 \theta_0^-} \times \frac{\mu}{\mu'} \left[\sin^2 \theta_0^- - \sin^2 \theta_c + \left(\frac{\mu'}{\mu} \right)^2 \cos^2 \theta_0^- \right] \quad (62)$$

where θ_0^- depends on the mode quantum numbers according to Eq. (54). In the usual case where $\mu \approx \mu'$, the second line of the formula simplifies to just $\cos^2 \theta_c$.

Obviously, when θ_0^- approaches θ_c , which would occur at weak enough index mismatch, the estimated lifetime $\tau_{\text{TM}} \rightarrow 0$, which is the limit of a non-bound state. At the opposite extreme of large index mismatch where $n/n' \gg 1$, this estimate varies as $1/\cos^2 \theta_0^-$, and since $\omega a/c^*$ is a number of order unity, the order of magnitude is determined by

$$\tau_{\text{TM}} \sim \frac{a}{c} \sqrt{\epsilon \mu}. \quad (63)$$

The result is interesting because it shows a lifetime that increases with the triangle size, as well as being proportional to the refractive index in the cavity.

For **TE polarization**, with $\psi = B_z$, the exterior magnetic field of a single evanescent wave has only a z -component like that in Eq. (II A). The calculation follows the same reasoning as used for the TM modes, but the specific details lead to a slightly different result. Definition of the Poynting vector as in (59) is the same. The substitution $|\vec{E}'| = |B'_z|/\sqrt{\epsilon'\mu'}$ together with Eq. (II A) for B'_z , followed by $|E_i^0| = |B_i^0|/\sqrt{\epsilon\mu}$ within the cavity, leads to the boundary wave power with extra factors,

$$P_x = \frac{ch}{4\pi\mu'} \frac{\mu' \epsilon |E_i^0|^2}{\omega/c} \frac{n \sin \theta_i}{\sqrt{(n \sin \theta_i)^2 - (n')^2}} \cos^2 \frac{\alpha}{2} \quad (64)$$

where now the phase shift α given by (16) in Sec. II A depends on the ratio $\epsilon/\epsilon' \gg 1$ rather than $\mu/\mu' \approx 1$. Furthermore, using (52) and (48), the energy stored in the cavity fields is now

$$U_{\text{TE}} = \frac{h}{8\pi\mu} \frac{3\sqrt{3}}{8} a^2 |\mathcal{A}_0|^2. \quad (65)$$

With cavity magnetic field strength $|B_i^0|^2 = \frac{1}{4} |\mathcal{A}_0|^2$, and again estimating the lifetime using only the ψ_0^- boundary wave from all three edges, the lifetime is $\tau_{\text{TE}} \approx U_{\text{TE}}/3P_x$. One finds

$$\omega \tau_{\text{TE}} \approx \frac{\sqrt{3}}{4} \left(\frac{\omega a}{c^*} \right)^2 \frac{\sqrt{1 - (\sin \theta_c / \sin \theta_0^-)^2}}{\cos^2 \theta_0^-} \times \frac{\epsilon}{\epsilon'} \left[\sin^2 \theta_0^- - \sin^2 \theta_c + \left(\frac{\epsilon'}{\epsilon} \right)^2 \cos^2 \theta_0^- \right]. \quad (66)$$

The second line of this formula highlights the difference for TE polarization compared to TM. The factor in the brackets is some number less than 1; it contrasts the bracket which reduces to $\cos^2 \theta_c$ in formula (62) for the TM polarization lifetime when $\mu = \mu'$. The crucial difference is the factor $\epsilon/\epsilon' \gg 1$ present here, compared to a similar factor $\mu'/\mu \approx 1$ for the TM lifetime formula. This is the more dominant factor, and it suggests that roughly speaking, the ratio of the lifetimes for the

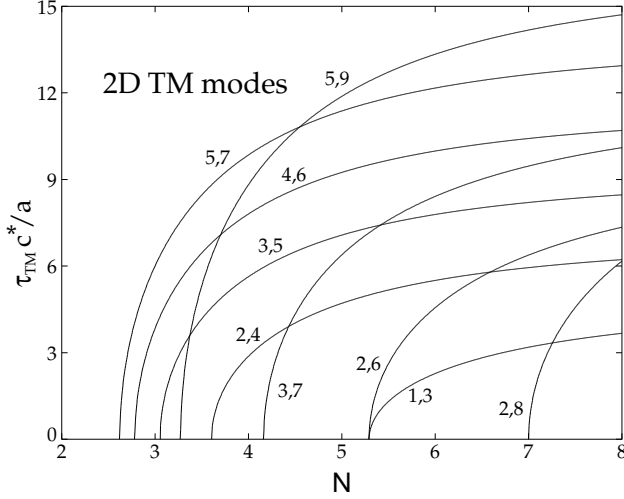


FIG. 10: Estimated lifetimes for some low TM modes indicated by (m, n) pairs, versus the index ratio N . The lifetime is scaled by the speed of light c^* in the cavity medium and the cavity edge size a .

two polarizations, which have the same (approximately DBC) boundary conditions and frequencies, is

$$\frac{\tau_{TE}}{\tau_{TM}} \approx \frac{\epsilon}{\epsilon'} = \left(\frac{n}{n'}\right)^2. \quad (67)$$

The result holds as long as the index mismatch is adequately large compared to the cutoff value needed to stabilize that mode by TIR. Otherwise, at smaller index mismatch, the TM lifetime can be longer than the TE lifetime.

Some results for τ_{TM} are presented in Fig. 10, showing lifetimes as functions of the index mismatch for some of the lowest modes. When scaled by the triangle size and light speed in the cavity, the lifetimes increase abruptly above the TIR confinement limits, eventually increasing at a slower rate. For the modes shown, dimensionless frequencies $\omega a/c^*$ are typically numbers greater than 10 (see Fig. 2), with the values of $\tau c^*/a$ also of the order of 10. Combining these rough results, the mode lifetimes in units of the mode periods T are similar to

$$\frac{\tau}{T} = \frac{\omega\tau}{2\pi} \sim \frac{10 \times 10}{2\pi} \approx 16. \quad (68)$$

Assuming that the lifetime estimates have included the dominant loss mechanism in the cavity, this large result for τ/T indicates that the original assumption of a resonance mode weakly confined by TIR should be a valid concept. Obviously, this holds far enough above the TIR confinement limits only, keeping in mind the approximate nature of the Dirichlet boundary conditions that were applied.

Comparative results for τ_{TE} for the same mode indexes are shown in Fig. 11. Due to the presence of the extra factor of $\epsilon/\epsilon' \approx N^2$, these lifetimes increase much more

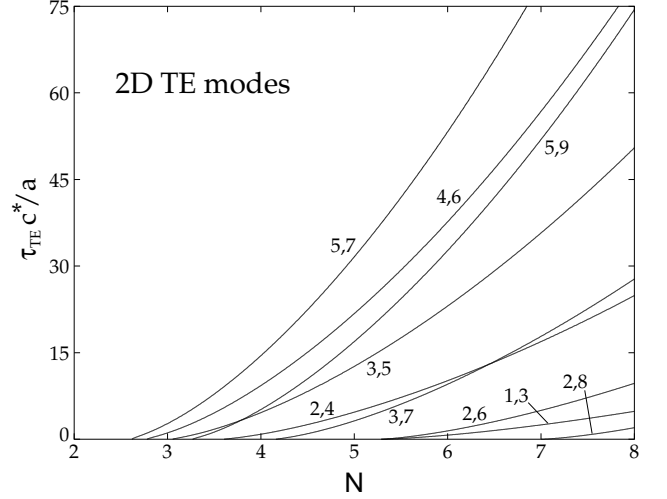


FIG. 11: Estimated lifetimes for low TE modes indicated by (m, n) pairs, versus the index ratio N . These lifetimes are larger than the corresponding TM lifetimes (Fig. 10) when N is sufficiently larger than the cutoff value for that mode.

rapidly than the TM lifetimes. As an example, for mode (3, 5), the TE lifetime is about 6 times longer than the TM lifetime at $N = 8$. On the other hand, for the mode (1, 3), which has a much larger TIR confinement limit, the TE lifetime is only about 1/3 longer than the TM lifetime at $N = 8$. Clearly, modes with (m, n) indexes nearly the same, as in the form $(m, m + 2)$ with large m , require smaller index mismatch for TIR confinement, and will more closely follow the lifetime ratio determined strongly by the index mismatch, Eq. (67).

In recent experiments[2] triangular semiconductor cavities with edges ranging from 75 to 350 μm were used. Assuming an effective index of refraction around $n \approx 4$, with vacuum on the exterior, and using $a \approx 100\mu\text{m}$, Eqs. (63) and (67) give rough lower estimates $\tau_{TM} \sim 1.3$ ps, and $\tau_{TE} \sim 20$ ps. Of course, for practical purposes of maintaining a resonating mode, a large value of τ/T is much more relevant, as discussed above. Based on these calculations, smaller cavities will have reduced lifetimes, but also shorter oscillation periods in the same ratio. For large index ratio, where $\sin \theta_c \ll 1$, $\cos \theta_c \approx 1$, and using the fact that $m < n$, lifetime expression (62) and frequency expression (28) produce the quality factor estimate,

$$Q = 2\pi \frac{\tau_{TM}}{T} \approx \frac{\pi^2 n^2}{\sqrt{3}}. \quad (69)$$

This ratio is independent of the cavity size or dielectric properties, increasing only with the squared mode quantum number n . The TE mode lifetime under these assumptions should be even larger, by the squared refractive index ratio $(n/n')^2$.

V. CONCLUSIONS

The resonant modes of an optical cavity with an equilateral 2D cross-section have been examined in an approximate manner, starting from the exact analytic solutions for Dirichlet boundary conditions. The six plane waves that make up each mode have been analyzed for the conditions necessary such that all are confined in the cavity by TIR. For 2D electromagnetics ($k_z = 0$), modes with larger ratios of quantum indexes m/n are most easily confined; conversely, modes with $m = 0$ never undergo TIR confinement. The presence of a nonzero longitudinal wavevector k_z can be expected to improve the possibilities for TIR confinement.

The critical index ratios for TIR confinement are the same for TM and TE polarizations. The different Fresnel factors, however, produce different rates of energy lost from the cavity by the evanescent boundary waves. For the 2D problem, this was shown to lead to considerably longer lifetimes of the TE polarization, enhanced approximately by a factor of the squared index ratio $(n/n')^2$ compared to the TM lifetime. The differences in these lifetimes would be expected to imply stronger coupling of EM fields from outside to inside the cavity in the TM polarization; it suggests that stimulation and generation of the modes by an external light source should be more efficient for TM polarization.

-
- [1] S. L. McCall, A. F. J. Levi, R. E. Slusher, S. J. Pearton, and R. A. Logan, *Appl. Phys. Lett.* **60**, 289 (1992).
 - [2] H. C. Chang, G. Kioseoglou, E. H. Lee, J. Haetty, M. H. Na, Y. Xuan, H. Luo, A. Petrou, and A. N. Cartwright, *Phys. Rev. A* **62**, 013816 (2000).
 - [3] A. W. Poon, F. Courvoisier, and R. K. Chang, *Opt. Lett.* **26**, 632 (2001).
 - [4] C. Y. Fong and A. W. Poon, *Optics Express* **11**, 2897 (2003).
 - [5] H.-J. Moon, K. An, and J.-H. Lee, *Appl. Phys. Lett.* **82**, 2963 (2003).
 - [6] U. Vietze, O. Krauß, F. Laeri, G. Ihlein, F. Schüth, B. Limburg, and M. Abraham, *Phys. Rev. Lett.* **81**, 4628 (1998).
 - [7] I. Braun, G. Ihlein, F. Laeri, J. U. Nöckel, G. Schulz-Ekloff, F. Schüth, U. Vietze, O. Weiß, and D. Wöhrle, *Appl. Phys. B: Lasers Opt.* **B 70**, 335 (2000).
 - [8] S. Bidnyk, B. D. Little, Y. H. Cho, J. Krasinski, and J. J. Song, *Appl. Phys. Lett.* **73**, 2242 (1998).
 - [9] H. X. Jiang, J. Y. Lin, K. C. Zeng, and W. Yang, *Appl. Phys. Lett.* **75**, 763 (1999).
 - [10] H. X. Jiang, J. Y. Lin, K. C. Zeng, and W. Yang, *Appl. Phys. Lett.* **74**, 1227 (1999).
 - [11] J. Wiersig, *J. Opt. A: Pure Appl. Opt.* **5**, 53 (2003).
 - [12] M. G. Lamé, *Leçons sur la théorie mathématique de l'élasticité des corps solides* (Bachelier, Paris, 1852).
 - [13] H. R. Krishnamurthy, H. S. Mani, and H. C. Verma, *J. Phys. A: Math. Gen.* **15**, 2131 (1982).
 - [14] C. Itzykson and J. M. Luck, *J. Phys. A: Math. Gen.* **19**, 211 (1986).
 - [15] M. Brack and R. K. Bhaduri, *Semiclassical Physics* (Addison-Wesley Frontiers in Physics, 1997).
 - [16] M. Brack, J. Blaschke, S. C. Creagh, A. G. Magner, P. Meier, and S. M. Reimann, *Z. Phys. D* **40**, 276 (1997).
 - [17] J. A. de Sales and J. Florencio, *Phys. Rev. E* **67**, 016216 (2003).
 - [18] J. D. Jackson, *Classical Electrodynamics* (John Wiley and Sons, New York, 1975), 2nd ed.
 - [19] E. Gutkin, *Physica* **19D**, 311 (1986).
 - [20] R. L. Liboff, *J. Math. Phys.* **35**, 596 (1994).
 - [21] L. Molinari, *J. Phys. A: Math. Gen.* **30**, 6517 (1997).
 - [22] O. Frank and B. Eckhardt, *Phys. Rev. E* **53**, 4166 (1996).
 - [23] J. Wiersig, *Phys. Rev. A* **67**, 023807 (2003).